POLITECNICO
MILANO 1863

SCUOLA DI INGEGNERIA INDUSTRIALE
E DELL'INFORMAZIONE

Executive Summary of the Thesis

Satellite manoeuvre detection and estimation with radar observations

Laurea Magistrale in Space Engineering - Ingegneria Spaziale

Author: Lorenzo Porcelli

Advisor: Prof. Pierluigi Di Lizia

Co-advisor: Dr. Diego Escobar Antón

Academic year: 2021-2022

1. Introduction

The increasing number of Resident Space Objects (RSOs) and congestion of the orbital debris environment cause activities for cataloguing of space objects to become more challenging year after year. The main source of potential new object detection corresponds to manoeuvres of operational satellites [1], which cause those satellites to be in orbits unexpected by cataloguing systems. Detecting manoeuvres is crucial for maintaining catalogues of RSOs, since otherwise **duplication of objects** and **degradation of the precision** of the orbital states might occur. Both these effects lead to a loss in accuracy of catalogues, which is reflected on the overall quality of the services provided by a SST operator. The consequences might be even extremely dangerous: as example, high-risk collision events might not be predicted sufficiently in advance or re-entry analyses might be completely imprecise.

2. Scope of the thesis

The **scope of the thesis** is to present a novel and operationally feasible methodology for manoeuvre detection and estimation, which shall be included as part of maintenance chain for RSOs. The methodology is conceived for a foreseen real time application, so particular care is given to its computational efficiency. Manoeuvre detection and estimation are posed as a track-to-orbit association problem between the orbit of an RSO, estimated some days before the manoeuvre, and a set of uncorrelated tracks, received afterwards. Manoeuvre estimation is a **two-step process**:

1. starting from the UCTs and the pre-manoeuvre orbit, a **first guess** for the manoeuvre is estimated employing a batch-least squares parameter estimation method with a simple dynamical model.
2. a **refined** manoeuvre estimation and post-manoeuvre orbit are computed via high-fidelity batch least-squares orbit determination.

Due to the impact of the manoeuvre on orbital dynamics, most post-manoeuvre tracks will not be correlated against any object in the catalogue. Such tracks, if compared to the pre-manoeuvre orbit in the measurements space, can show high residuals. Hence, the latter are employed in the detection strategy, where the occurrence of a manoeuvre is determined when certain thresholds are exceeded. The potential manoeuvre is estimated at first by following an optimal control approach, where the velocity increase (i.e., a ΔV) is used within a cost function. This algorithm is an evolution, adaptation and extension of a methodology presented

by Pastor et. al [1]. Differently from the previous work, focused on the GEO regime, the work presented here targets LEO objects, subject to faster and more non-linear dynamics; to this aim, the development of an **improved propagation model** for the manoeuvre estimation process is presented with the goal of minimising the associated computational cost while maintaining reasonable accuracy for the LEO regime. This task represents of the major contributions of the following dissertation. The result of the estimation is a pool of possible solutions, from which a proper **a-priori estimate** is chosen according to a selection criterion based on the weighted errors of the residuals and on the control effort. The selection strategy is an evolution of the one proposed in GEO. Figure 1 presents a flow chart of the cataloguing maintenance phase, in which the role of the proposed algorithm to get the first manoeuvre estimate is highlighted.

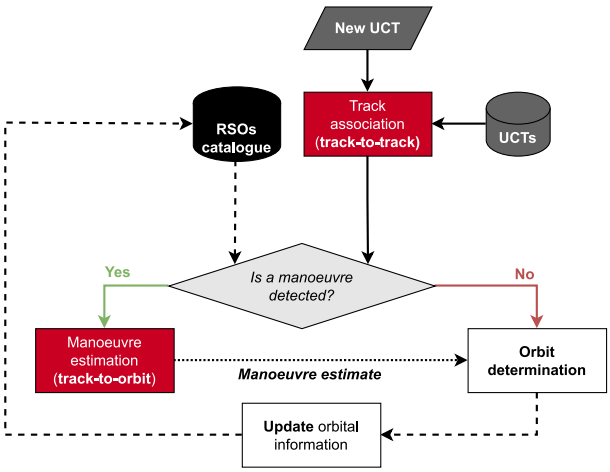

Figure 1: Catalogue maintenance accounting for manoeuvres.

The methodology is presented for a single-satellite scenario, considering just one RSO orbit and sets of tracks belonging to the very same object. Nonetheless, it can be trivially extended to a wider **multi-target association framework**. In fact, if one considers a typical surveillance scenario with multiple orbits, the estimated manoeuvres can represent a preliminary link, or hypothesis, established between the UCTs and the object. The union of these hypotheses builds up an association tree, which needs to be evaluated and pruned in order to finally promote the best correlation which connects the involved catalogued orbit and the processed observation data. The estimation of the post-manoeuvre orbit and the manoeuvre itself has mediocre accuracy if only measurements from a single post-manoeuvre track are used, losing the ability to associate future tracks. Hence, the track-to-orbit correlation process must be preceded by a track-to-track association step (developed by Pastor et al. [2]), used to cluster together enough post-manoeuvre tracks corresponding to the same RSO. This is of course trivial in scenarios where tracks are known to belong to the same object, but is a fundamental step in the multi-target multi-sensor association framework. The employment of the track-to-track association process allows to reach estimation accuracy analogous to no-manoeuvre scenarios if enough tracks are gathered. Tests are performed considering a simulation scenario including **radar tracks**, providing a clear understanding of the performances of the methodology and serving as a basis for the development of the multi-target association framework. Results are presented and discussed, emphasising the benefits and the limitations of the overall approach.

3. Methodology for manoeuvre detection and estimation

3.1. Manoeuvre detection

As a spacecraft performs impulsive manoeuvres, due to the change in the velocity, a divergence in the residuals with respect to the pre-manoeuvre orbit is expected to be noticeable. This divergence is sought in the measurements space, since a post-manoeuvre orbit cannot be reliably estimated from a single track [3]. Consider the pre-manoeuvre orbit under analysis (with subscript A), estimated with pre-manoeuvre tracks. The ephemerides of such orbit can be propagated with a high-fidelity numerical propagator in time defined by the variable t, computing the trajectory of an extended state vector as:

$$\mathbf{y}_A(t) = [\mathbf{x}_A(t), \mathbf{p}_A(t)] \in \mathbb{R}^{(6+n_p)} \qquad (1)$$

The first part of the vector, $\mathbf{x}_A(t) \in \mathbb{R}^6$, is the aggregation of the Cartesian position vector $\mathbf{r}_A(t) \in \mathbb{R}^3$ and velocity vector $\mathbf{v}_A(t) \in \mathbb{R}^3$. On the other hand, the vector $\mathbf{p}_A(t) \in \mathbb{R}^{n_p}$ is a set of dynamical parameters. Consider now a possible post-manoeuvre track. It can be de-

composed into a set of observations $\{\mathbf{z}_k\}$, where each $\mathbf{z}_k = \mathbf{z}(t_k)$ is a vector containing separate measurements taken at the observation times t_k for $k = 1, \ldots, K$, with K being the total number of observations in the track. The selected metric for manoeuvre detection is the **weighted root mean square residual** of each measurement type in the track with respect to the pre-manoeuvre orbit:

$$WRMS_i = \sqrt{\frac{1}{K}\sum_{k=1}^{K}\frac{\rho_{i,k}^2}{\sigma_i^2}} \tag{2}$$

where the index $i = 1, \ldots, I$ refers to the type of measurement. The term $\rho_{i,k} = z_{i,k} - \mathbf{h}(t_k, \mathbf{x}_A(t_k))$ represents the residual of the i-th type of measurement at the epoch of the k-th observation (t_k). The function $\mathbf{h}(t_k, \mathbf{x}_A(t_k))$ is an analytical model to reconstruct measurements starting from the state vector of the pre-manoeuvre orbit. The denominators σ_i are the standard deviations of the measurements, quantifying the expected 1-sigma noise of the sensor for a given measurement type. A manoeuvre is expected to have occurred if the WRMS of a single track crosses a **threshold** called absolute WRMS threshold. The selection of its value descends from a trade-off: the threshold should be sufficiently low to trigger true manoeuvre detection, but also sufficiently high to discard any possible outlier and avoid false manoeuvre detection. A challenging case for this approach is encountered when, in the case of low magnitude burns, the first post-manoeuvre track arrives closely to the manoeuvre epoch. As only a short time period after the manoeuvre has passed, the divergence of the observations could be not sufficiently high to overpass the threshold. The robustness of the strategy is improved with the application of a **secondary threshold** (as opposed to the **primary threshold**): if a post-manoeuvre track is detected through the primary threshold, the algorithm looks to the past to find tracks that exceed the secondary threshold. Since these past tracks are supposed to show a smaller divergence with respect to the one detected with the primary threshold, the value of the secondary threshold should be lower than the primary.

3.2. Manoeuvre estimation

The manoeuvre detection scheme provides a set of tracks which are labelled as post-manoeuvre. These can be decomposed into the observations $\{\mathbf{z}_l\}$, where each $\mathbf{z}_l = \mathbf{z}(t_l)$ contains all the measurements taken at the observation times t_l for $l = 1, \ldots, L$, with L being the total number of observations in all tracks. At a certain epoch, defined as t_M, an impulsive manoeuvre is assumed to take place. The pre-manoeuvre orbit $\mathbf{x}_A(t)$ will therefore drift towards $\mathbf{x}_B(t, \mathbf{u})$, named post-manoeuvre orbit (or also orbit B). Given the hypothesis of impulsive burn, the two orbits intersect at t_M: their position vectors are the same, while the difference in velocity is given by the manoeuvre $\mathbf{u} \in \mathbb{R}^3$, such that $\mathbf{v}_B(t_M) - \mathbf{v}_A(t_M) = \mathbf{u}$. The manoeuvre $\mathbf{u}$ occurring at t_M is found as the one that minimises the residuals of the true observations $\{\mathbf{z}_l\}$ with respect to the post-manoeuvre orbit $\mathbf{x}_B(t, \mathbf{u})$ (as represented in Figure 2). This methodology was already developed for manoeuvre estimation of GEO objects [1].

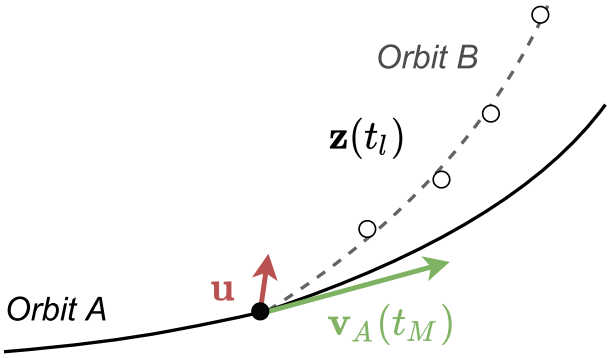

Figure 2: Graphical representation of the manoeuvre estimation method.

This is equivalent to a **parameter estimation problem** using $\mathbf{u}$ as solve-for parameters, while keeping t_M fixed to a given value, as it was proven that a joint estimation is unsatisfactory due to the non-linearities of the problem [1]. The residuals at each observation time t_l can be computed as $\boldsymbol{\rho}_l = \mathbf{z}(t_l) - \mathbf{h}(t_l, , \mathbf{x}_B(t_l, \mathbf{u}))$, which is a vector of dimension equal to the number of considered measurement types (denoted as I). The goal is to find the manoeuvre which best fits the observations in a least-squares of the residuals sense. This is achieved by minimising the following cost function:

$$J = \frac{1}{L}\sum_{l=1}^{L} \boldsymbol{\rho}_l^T W \boldsymbol{\rho}_l \tag{3}$$

The matrix $W \in \mathbb{R}^{I\times I}$ is the **weighting matrix**, which accounts for the expected errors of the measurements and puts into effect the non-dimensionalisation of the residuals. Assuming that the errors are non-correlated, W is a diagonal matrix with its components being the squared inverse of expected uncertainties σ_i of the measurements. The cost function might be rewritten by considering a linearisation of the residuals with respect to a reference value for the manoeuvre $\mathbf{u}^*$ [4], which becomes then a function of the **correction** $\Delta\mathbf{u}$. The search for the minimum of J results in the following **normal equations**, solved iteratively with the initial solution $\mathbf{u}^* = \mathbf{0}$ (updated at each step):

$$(G^T W G)\,\Delta\mathbf{u} = (G^T W)\,\Delta\mathbf{z} \tag{4}$$

The term $\Delta\mathbf{z} = \sum_l \mathbf{z}_l - \mathbf{h}\left(t_l,\, \mathbf{x}_B\left(t_l,\, \mathbf{u}^*\right)\right) \in \mathbb{R}^I$ represents the difference between the true measurements and those reconstructed from the reference trajectory $\mathbf{x}_B^*(t_l) = \mathbf{x}_B\left(t_l,\, \mathbf{u}^*\right)$. The term $G \in \mathbb{R}^{I\times 3}$ is instead the **Jacobian**, which represents the partial derivatives of the measurements with respect to the estimated parameters. It can be computed as a sum of the contributions of each observation:

$$\begin{aligned} G &= \sum_l \frac{\partial \mathbf{h}\left(t_l,\, \mathbf{x}_B\left(t_l,\, \mathbf{u}^*\right)\right)}{\partial \mathbf{u}} \\ &= \sum_l \frac{\partial \mathbf{h}\left(t_l,\, \mathbf{x}_B\left(t_l,\, \mathbf{u}^*\right)\right)}{\partial \mathbf{x}_B\left(t_l,\, \mathbf{u}\right)} \cdot \frac{\partial \mathbf{x}_B\left(t_l,\, \mathbf{u}^*\right)}{\partial \mathbf{u}} \end{aligned} \tag{5}$$

3.3. Selection of first manoeuvre estimate for subsequent re- estimation

The normal equations must be solved for a set of t_M values comprised in an interval T (from the last track used to estimate the pre-manoeuvre orbit to the first post-manoeuvre track being considered). Hence, the output of the algorithm is a pool of solutions for every $t_M \in T$, each one associated to a WRMS and to an estimated manoeuvre $\hat{\mathbf{u}}$. A simple strategy is proposed to retrieve the most suitable **a-priori estimate** (that is a combination of $\hat{t}_M$ and $\hat{\mathbf{u}}$):

1. the global minimum in terms of WRMS (Equation (3)) is detected and then just the solutions with a value of $\sqrt{J}$ **lower than the 115%** of the minimum are retained.
2. among this set, the solution associated to the **lowest control effort** $\|\hat{\mathbf{u}}\|$ (with $\|(\cdot)\|$ representing the norm of a vector) is eventually selected.

$\sqrt{J}$ is selected as the leading metric for the short-listing as it quantifies the quality of the estimation. The rationale behind second step in the selection strategy is that manoeuvres performed by satellites are normally designed to be optimal. The current percentage value for taking the solutions with minimum WRMS has proven to be a reasonable value, as it allows to locate the local minima regions and to account for the errors introduced by the discretization of T. The selection criterium is slightly different from the previous one [1], where the best solution was taken as the one with lowest $\|\hat{\mathbf{u}}\|$ but just among the local WRMS minima, without considering any margin for enlarging the pool. It is important to remark that this selection strategy is intended to be as simple as possible at deriving a reliable first estimate and is tailored to a single-satellite scenario. Further developments, aimed at extending the correlation problems to multiple RSOs, shall be posed in a multi-target association framework. Once that the a-priori estimates for the manoeuvre time and guess have been found as described above, it is possible to perform a high-fidelity orbit determination process, with a numerical propagator, which determines the post-manoeuvre orbit and refines the initial guesses.

3.4. Development of a dynamical model for manoeuvre estimation

The last step required to complete the manoeuvre estimation algorithm is to define a dynamical model for $\mathbf{x}_B\left(t,\, \mathbf{u}\right)$, required for the computation of the predicted measurements and of the matrix G. The requirement of computing multiple solutions for a set of t_M values before the final selection imposes a requirement to have a computationally efficient propagation algorithm. For this reason, a simple, fast and yet sufficiently accurate dynamical model partially based on linear dynamics is developed. The model is an improvement of the fully-

linear one employed in manoeuvre estimation of GEO objects [1]. A product of the orbit determination process and propagation of the pre-manoeuvre trajectory is the **state transition matrix** $\Phi(t, t_0)$, estimated with respect to a reference time t_0. This matrix represents the linear mapping between the initial state vector $\mathbf{x}_A(t_0)$ and the state vector at any time t:

$$\Phi(t,\, t_0) = \frac{\partial\, \mathbf{x}_A(t)}{\partial \mathbf{x}_A(t_0)} \in \mathbb{R}^{6\times 6} \tag{6}$$

The post-manoeuvre trajectory of $\mathbf{x}_B(t)$ can be found from a Taylor expansion with respect to a reference, taken equal to $\mathbf{x}_A(t)$, and retaining the zero and first order terms:

$$\mathbf{x}_B(t) \approx \mathbf{x}_A(t) + \frac{\partial \mathbf{x}_A}{\partial \mathbf{x}_A^0}(t) \cdot \left(\mathbf{x}_B^0 - \mathbf{x}_A^0\right) \tag{7}$$

where $\mathbf{x}_A^0$ and $\mathbf{x}_B^0$ are the considered initial state of the two trajectories. Considering the beginning of the propagation at $t = t_M$, which is the manoeuvre epoch, the post-manoeuvre state can be simply obtained through the derivative $\partial \mathbf{x}_A / \partial \mathbf{x}_A^0$ (which is the STM of orbit A referred to t_M, namely $\Phi(t,\, t_M)$) and the difference between the initial states, equal to the manoeuvre $\mathbf{u}$, since:

$$\mathbf{x}_A^0 = \mathbf{x}_A(t = t_M) \tag{8}$$

$$\mathbf{x}_B^0 = \mathbf{x}_B(t = t_M,\, \mathbf{u}) = \mathbf{x}_A^0 + [\mathbf{0},\, \mathbf{u}]^T \tag{9}$$

Separating the contributions due to the central motion and due to perturbations in the STM, and retrieving the Keplerian dynamics in its full linearity, the final expression of $\mathbf{x}_B(t,\, t_M,\, \mathbf{u})$ can be written as:

$$\begin{aligned}\mathbf{x}_B(t,\, t_M,\, \mathbf{u}) &= \mathbf{x}_A(t) + \\ &+ \left[\mathbf{x}_{B,K}(t,\, t_M,\, \mathbf{u}) - \mathbf{x}_{A,K}(t,\, t_M)\right] + \\ &+ \left[\Phi(t,\, t_M) - \Phi_K(t,\, t_M)\right]_{\mathbf{xv}} \cdot \mathbf{u}\end{aligned} \tag{10}$$

The subscripts $(\cdot)_{\mathbf{xv}}$ represents the submatrices of the partial derivatives with respect to just the velocity components, as the difference in the two initial states does not have any position component. The term $[\mathbf{x}_{B,K}(t,\, t_M,\, \mathbf{u}) - \mathbf{x}_{A,K}(t,\, t_M)]$ represents the difference between two fully non-linear Keplerian trajectories, propagated from the initial states in Equations (8) and (9). The matrix $\Phi_K(t,\, t_M)$ is instead the state transition matrix related to $\mathbf{x}_{A,K}(t,\, t_M)$, computed via a numerical scheme (2^{nd} order central differences). In the former work by Pastor [1], the dynamical model for describing the post-manoeuvre trajectory considered both the Keplerian motion and the perturbations under linear dynamics:

$$\mathbf{x}'_B(t,\, t_M,\, \mathbf{u}) = \mathbf{x}_A(t) + \Phi(t,\, t_M)_{\mathbf{xv}} \cdot \mathbf{u} \tag{11}$$

Having derived the equation of the dynamical model, it is required to define an expression for $\partial \mathbf{x}_B(t,\, \mathbf{u}) \,/\, \partial \mathbf{u}$ (for a fixed t_M) to build up the contributions to the normal equations matrix (Equation (5)). Differentiating Equation (10) with respect to $\mathbf{u}$:

$$\begin{aligned}\frac{\partial \mathbf{x}_B(t, \mathbf{u})}{\partial \mathbf{u}} = \frac{\partial \mathbf{x}_{B,K}(t, \mathbf{u})}{\partial \mathbf{u}} + \\ + \left[\Phi(t, t_M) - \Phi_K(t,\, t_M)\right]_{\mathbf{xv}}\end{aligned} \tag{12}$$

The first term on the right-hand side is the state transition matrix of the Keplerian trajectory $\mathbf{x}_{B,K}(t,\, \mathbf{u})$, since a variation of $\mathbf{u}$ directly implies a variation on the initial state $\mathbf{x}_B^0$. The reason behind the development of this enhanced version of the linear model, which will also be referred to as **Keplerian + linear perturbations model** (Equation (10)), is the foreseen application in LEO, where dynamics are faster and subject to higher non-linearities if compared to the GEO environment.

4. Results

4.1. Results of the accuracy tests for the dynamical models

The presented dynamical model is tested to define its performances. It is compared against a high-fidelity numerical propagator, to determine the level of error reached in the propagation, and against the linear propagator previously employed for manoeuvre detection of GEO objects, to assess the benefits of using this newly developed model. The subject of the tests is a LEO object, whose characteristics are reported in Table 1. The orbit of the satellite is propagated for a total of 5 days, considering a manoeuvre to happen after 1 day of simulation.
To begin with, two high-fidelity propagations is performed. The force contributions included

Epoch	September 5th, 2018, 00:00
Position r	$[3528.52, -4599.69, 4232.54]^T$ km
Velocity v	$[-3.72, 2.59, 5.91]^T$ km/s
Mass	$1000\,kg$
Area	$10\,m^2$
Drag coeff.	3.334
SRP coeff.	0.967

Table 1: Characteristics of satellite for propagation accuracy test.

in the dynamical model are reported in Table 2. The propagation generates the trajectory of $\mathbf{x}_A(t)$, required for both the linear and the Keplerian + linear perturbations models. The second one, considering an impulsive manoeuvre equal to $[10, 10, 10]^T$ cm/s in the Radial – In-track – Cross-track (RIC) frame, generates $\mathbf{x}_B^{num}(t)$ (which is taken as a reference for comparison). The two linearised dynamical models are used to compute two trajectories considering the same manoeuvre. The results of the test are presented in the plot through the Root Mean Square Error (RMSE), divided in position and velocity components, of the difference between the high-fidelity and the approximated trajectories, namely the RMSE of $\mathbf{x}_B^{num} - \mathbf{x}_B$ and of $\mathbf{x}_B^{num} - \mathbf{x}'_B$. The difference in the position components is defined as $\Delta\mathbf{r}$, while the one for the velocity components is $\Delta\mathbf{v}$. The errors are averaged in rolling mean over time windows approximately equal to an orbital revolution of the satellite (computed at t_M after the manoeuvre). In each of the plots, the vertical dashed line represents the manoeuvre epoch. An important difference in the performances of the two models can be observed. Errors reach up to 700 m and 0.8 m/s for the linear model, while $\approx$ 400 m and 0.4 m/s for the other one. It is also noticeable that the propagation with the Keplerian + linear perturbations model starts diverging approximately one day later than the other one.

4.2. Setup of simulation scenario

The combined manoeuvre detection and estimation algorithm is tested by setting up a simulation scenario resembling a cataloguing maintenance chain. The subject of the tests is **Sentinel 3-A**, which is on a low-eccentricity polar orbit, with a nominal altitude of 814 km and inclination of 98.65°. The time window considered for the simulation starts in 2017 and ends in 2019. The satellite performs a total of 22 manoeuvres, with burn magnitude varying from a few mm/s to m/s. Manoeuvres are either impulsive, with duration in the order of a few seconds, or long, with duration between 12 and 15 minutes. Both the initial orbit and manoeuvre history are publicly available [5] [6]. With such manoeuvre history, an orbit is propagated for the three years and simulated tracks are generated considering one radar located in mainland Spain, having a pyramidal field of view with 43.2° × 30° in semi-aperture. The noise is added to each observation in the tracks as a random number picked from a Gaussian distribution function with standard deviations equal to 10 m for 2-way range, 1000 mm/s for 2-way range rate and 300 $mdeg$ for angular measurements.
The simulation is run by considering observation windows composed of 18 successive tracks each. Consecutive windows are shifted by just 1 track, in order to be able to analyse the effect of single tracks. The workflow resembles the scheme reported in Figure 1. For each window, the manoeuvre detection strategy is applied and if **post-manoeuvre tracks are discovered**, the estimation algorithm is run. If the manoeuvre is estimated with **up to 3 post-manoeuvre tracks**, the estimates are just stored as they are not considered to be fully reliable. On the other hand, if a manoeuvre is estimated with associations of **4 post-manoeuvre tracks** (enough to estimate a full orbit [3]), the estimates are deemed to be reliable, and the manoeuvre is considered to be confirmed. The a-priori estimate is used to compute a post-manoeuvre orbit via batch-least squares orbit determination (employing the numerical propagator reported in Table 2). The manoeuvre itself, in its components and epoch, is added as a **dynamical parameter to be re-estimated** (along with the state vector of the satellite). The selection of 4 as the number of post-manoeuvre tracks for a manoeuvre to be confirmed is suggested from the analysis of the test cases. This is in-line with the results of literature regarding track-to-track associations [3], which states that 3 or 4 tracks are usually sufficient to obtain correct correlations.

Gravity field	30 × 30
Atmospheric drag	MSISE90 model
Moon gravity	Third body perturbation + $J2$ gravity interaction
Third body perturbations	Sun and other planets
Planetary tides	Solid tides only
Solar radiation pressure	Cannonball model

Table 2: Force models of the high-fidelity propagator.

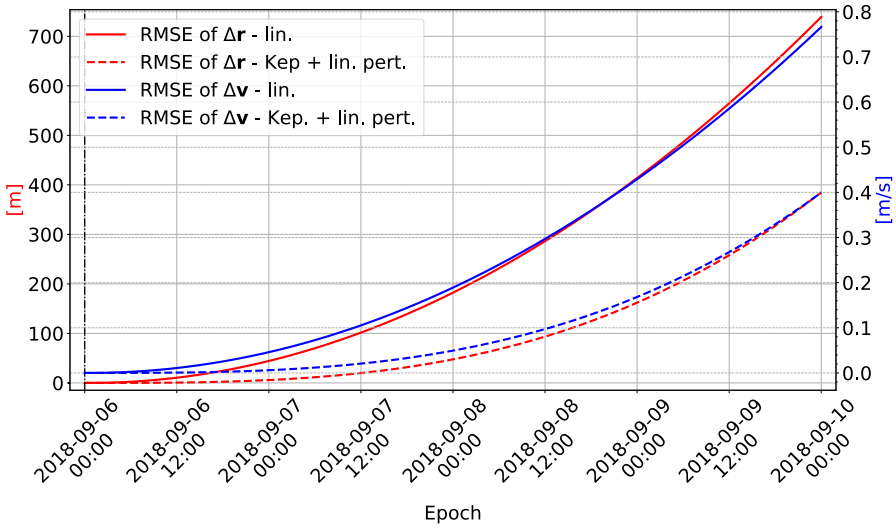

Figure 3: Results of the accuracy test for the dynamical models.

Good estimates could also be obtained with 2 tracks, but this proved to not be always the case. There are cases in which, after a manoeuvre is confirmed and estimated with 4 tracks, manoeuvre detection is triggered in the subsequent observation window, meaning that the WRMS of the post-manoeuvre orbit is still high and the estimation was not satisfactory. This situation occurs when the true manoeuvre that was tried to be estimated is a **long burn** (in the order of 10-15 minutes, which is a non-negligible portion of the orbital period). This occurrences are due to the limitations of the proposed manoeuvre estimation algorithm, which correlates the orbit to the tracks via an impulsive burn.

4.3. Results for manoeuvre detection

The primary and secondary thresholds to trigger manoeuvre detection are set to **5.0** and **2.5** respectively. For the application of the secondary threshold, it has been selected a maximum of **14 hours** to look for previous post-manoeuvre tracks. This value is slightly greater than the generic revisit time of a LEO satellite on a polar orbit. The following definitions are adopted:

1. the true manoeuvres which are correctly detected are labelled as **true positives**.
2. manoeuvres which do not occur but are still detected are named **false positives**.
3. true manoeuvres which are not detected are defined as **false negatives.**

The selection of these thresholds for the WRMS metric proves to be robust for manoeuvre detection. All 22 manoeuvres in the simulation time span are correctly detected, leading to 22 true positives and 0 false negatives. Even so, false positives are triggered in cases with long burn times, as the estimation of the post-manoeuvre orbit and of the manoeuvre itself, as already stated, can be poor and generate high track residuals. Some statistics regarding the performances of the manoeuvre detection strategy are reported through a confusion matrix in Figure 4. There are three cases where the first

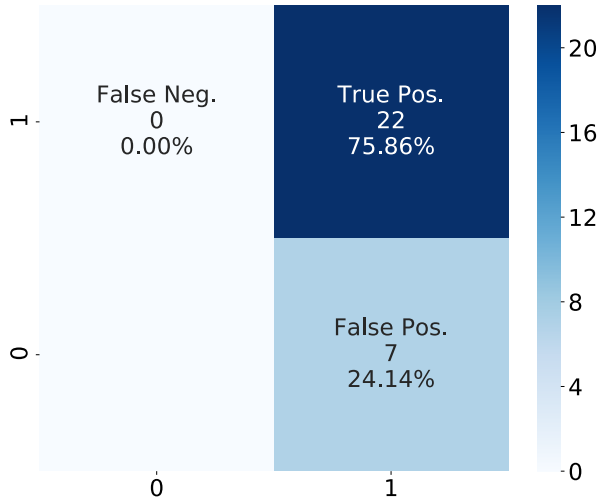

Figure 4: Confusion matrix for manoeuvre detection.

post-manoeuvre track is not immediately detected. This can be attributed to the fact that it arrives closely to the burn epoch and that the corresponding manoeuvre has relatively low magnitude. Nevertheless, the information about these observations are recovered and employed for manoeuvre estimation as soon as the second post-manoeuvre track, detected via the primary threshold, arrives, thanks to the application of the lower secondary threshold.

4.4. Results for maneovure estimation

In order to understand the general performances of the proposed two-step estimation methodology, this subsection presents an overview of the results obtained for the estimation of the 22 manoeuvres performed in years 2017, 2018 and 2019 by Sentinel 3-A. The two parameters which are considered to define the quality of the manoeuvre estimates are the errors in the estimated vector and the estimated epoch. Figures 5 to 8 report the distributions of the estimation errors of the epoch and of the relative manoeuvre magnitude error (knowing the true manoeuvres). The smaller graphs in each figure represent the distribution (and the Cumulative Distribution Functions) of the solutions according just to the magnitude error (on top) and the epoch error (on the right). The plots are presented for associations of an increasing number of post-manoeuvre tracks, from 1 to 4. Defining an association of post-manoeuvre tracks as a set of tracks {1, 2, 3, 4}, the associations in the distributions are {1}, {1, 2}, {1, 2, 3} and {1, 2, 3, 4}. The graphs on the top of each figure report the estimates coming from the estimation algorithm (using the Keplerian + linear perturbations dynamical model), while those below are the subsequent re-estimations of the first guesses employing high-fidelity orbit determination. The distributions on top sides show that, for an increasing number of post-manoeuvre tracks, the estimation error on both magnitude and epoch of the estimation algorithm tends to decrease, as well as the dispersion of the points. Associations of 1 track cannot be considered reliable since errors can reach very high values for both magnitude and epoch. The estimation is mediocre since a low number of measurements is involved and, at times, also because the track is received shortly after the manoeuvre. For associations of 2 tracks, errors can reach up to 200% in magnitude and 800 minutes in epoch, which drop to 75% and 150 minutes for 3 tracks, and finally to maximum 60% and 100 minutes for 4 tracks. This confirms the choice of 4 as the number of post-manoeuvre tracks to confirm a reliable first manoeuvre guess, since the errors are at their minimum and the dispersion of the points is the lowest among all associations; nonetheless, also associations 3 tracks can be eventually considered with a higher degree of uncertainty on the estimation. The outliers in terms of manoeuvre epoch are represented by long burns, which, as already stated, are not properly evaluated by the estimation algorithm and ambiguities in the selection of the first estimate arise. Associating more than 4 tracks could be beneficial but also lead to poor estimations, since the dynamical models (both the linear one and the Keplerian + linear perturbations) could start diverging for tracks far from the manoeuvre epoch in cases of higher magnitude burns. Moreover, the computational cost of the manoeuvre estimation algorithm would increase as more measurements should be processed. On the other hand, the distributions at the bottom, related to high-fidelity orbit determination, show how the estimation error and the dispersion can improve in the second iteration of estimation. It is possible to notice that, for all numbers of associated tracks, this step benefits both the error on magnitude and epoch, though having a greater impact on

the first one than on the second. This result was expected, as this estimation step is multi-parameter (since it considers both the manoeuvre vector and epoch) and is supported by a numerical propagator with higher fidelity.

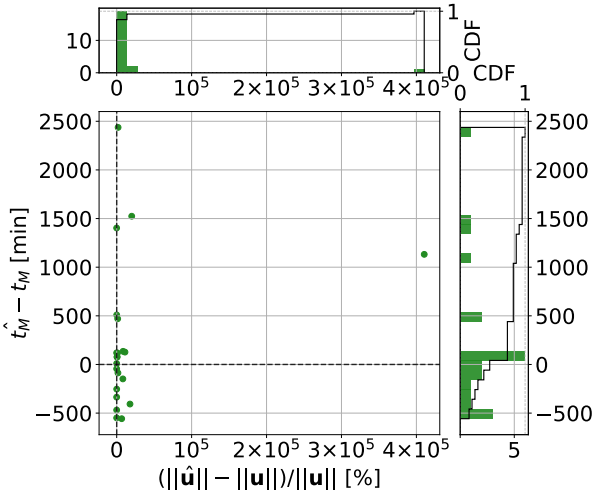

(a)

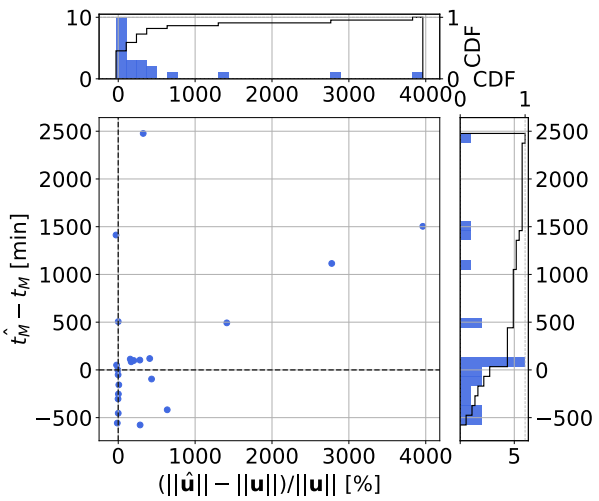

(b)

Figure 5: Distribution of manoeuvre estimates (top) with estimation algorithm and high-fidelity orbit determination (bottom) (*1 track*).

5. Conclusions

A novel approach for manoeuvre detection and estimation, conceived for an operational scenario, has been developed and tested for a single LEO satellite. The detection strategy is based on metrics that rely on the residuals of observations, while the estimation algorithm is a two-step process which employs parameter estimation at first and posterior high-fidelity orbit determination. The estimation algorithm requires the definition of a selection criterion to choose the most suitable guess among a set of different solutions. Results were presented and discussed for both the detection and estimation methodology. The first one was able to detect all the true manoeuvres, while false manoeuvre triggering was only encountered after the estimation of long burns. The manoeuvre estimation algorithm was tested with the Keplerian + linear perturbations dynamical model, whose aim is to increase accuracy while keeping the computational cost extremely low, as required when using this approach in a multi-target situation for association purposes. The newly developed

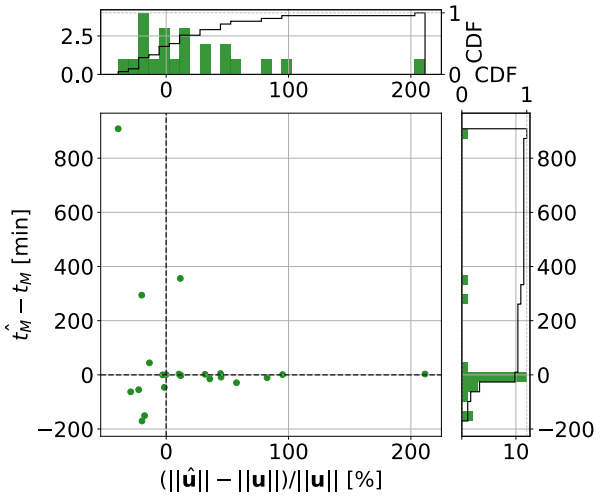

(a)

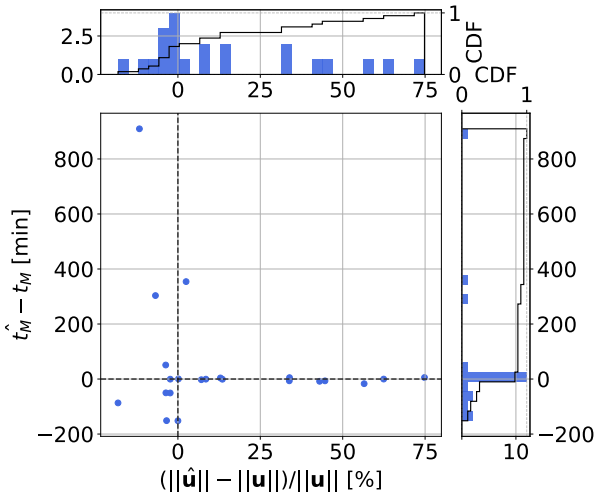

(b)

Figure 6: Distribution of manoeuvre estimates (top) with estimation algorithm and high-fidelity orbit determination (bottom) (*2 tracks*).

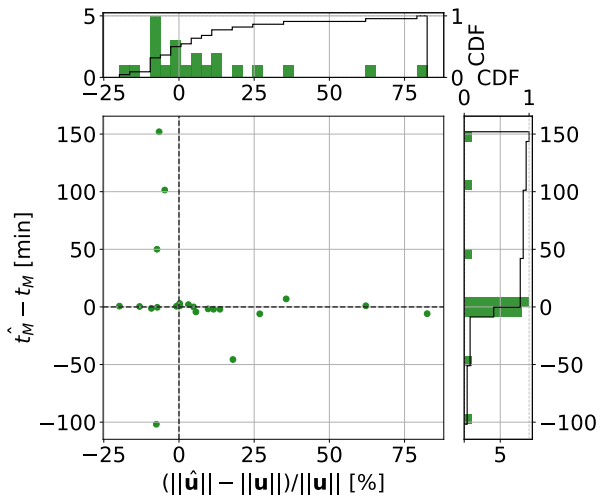

(a)

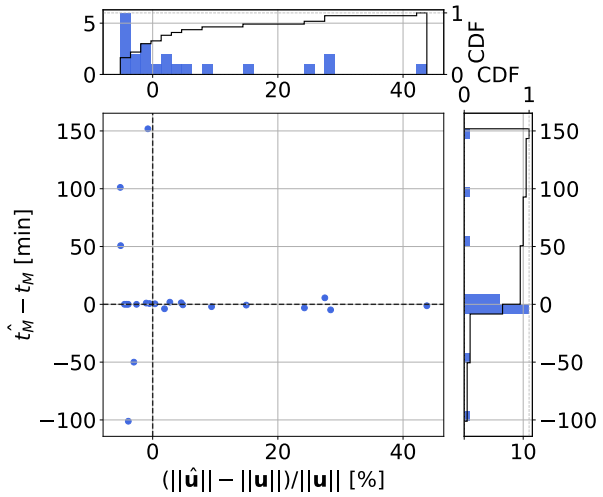

(b)

Figure 7: Distribution of manoeuvre estimates (top) with estimation algorithm and high-fidelity orbit determination (bottom) (*3 tracks*).

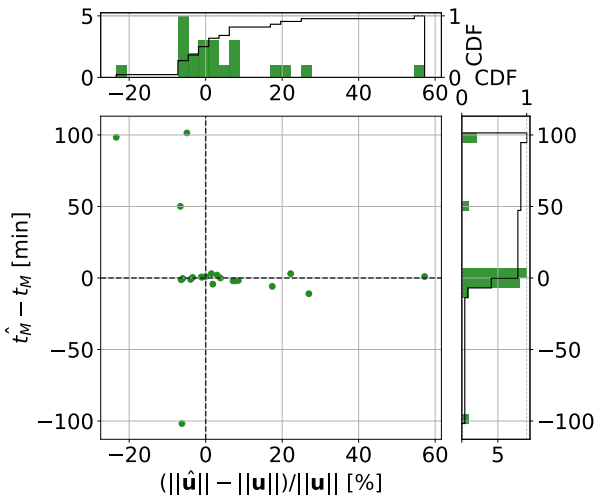

(a)

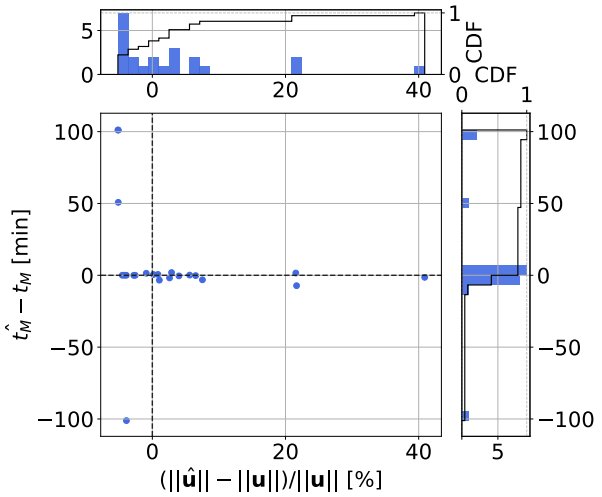

(b)

Figure 8: Distribution of manoeuvre estimates (top) with estimation algorithm and high-fidelity orbit determination (bottom) (*4 tracks*).

model is the major contribution of this work to the evolution of the work presented in [1]. The results of the two-step estimation process were presented. It was shown that the estimation algorithm, along with the selection criterion based on WRMS and on the control effort (adapted from the previous GEO analysis), can provide satisfactory results as the number of associated post-manoeuvre tracks increases. In this regard, it was proven that considering 3 or 4 tracks is a sound compromise between estimation quality and computational time; however, to have a safer margin, a manoeuvre is deemed to be confirmed only if estimated with 4 tracks in the simulation chain. Moreover, the impact of the second estimation step is able to increase the accuracy for both manoeuvre vector and epoch, validating the proposed approach. Future developments will be devoted to the extension of the track-to-orbit manoeuvre detection and estimation to a wider multi-target association framework, in which the goal will be to associate multiple manoeuvrable RSOs with their post-manoeuvre tracks. This task is challenging due the dimension and scalability of the problem, determined by every single combination of UCTs and objects without recently correlated tracks to compare. This can be relieved by the preliminary track-to-track association step and by setting up a consistent methodology to

discard most of unfeasible track-to-orbit correlations and build up an association tree considering manoeuvres. The detection strategy can be augmented by different metrics such as the median values of the WRMS, and by defining more secondary thresholds to increase robustness. Regarding the estimation algorithm, improvements can be achieved by increasing the accuracy of the propagation while keeping a relatively low computational effort. This can be done by including $J2$ as a perturbation term or a simple model for aerodynamic drag, as well as employing semi-analytical propagators. Finally, the author would like to mention that this thesis has been developed as part of an internship in the Space Situational Awareness section of the Flight Dynamics Operations and Systems business unit at GMV. This work will also be presented as a conference paper at the 3rd IAA Conference on Space Situational Awareness (ICSSA) in Madrid, Spain, on April 4th - 6th 2022.

6. Acknowledgements

At first, I would like to thank prof. Pierluigi Di Lizia, who followed and supported me throughout the development of the thesis, and to whom I'm grateful for proposing me the opportunity to work in a company abroad, allowing me to grow personally and begin a career in this sector. A word of thanks to Diego Escobar, head of the Space Situational Awareness section at GMV, who guided me in conducting the research and from whom I could learn a lot about these topics. A great thank you to Alejandro Pastor, who introduced me to these very interesting problems about data association and from whom I could take inspiration to develop the thesis. A special thanks to Alejandro Cano, who always provided me precious advice to improve this work and also grow professionally.

References

[1] A. Pastor et al. "Satellite maneuver detection and estimation with optical survey observations". In: *The Journal of the Astronautical Sciences* (2021). DOI: 10.1007/s40295-022-00311-5.

[2] A. Pastor, M. Sanjurjo-Rivo, and D. Escobar. "Track-to-track association methodology for operational surveillance scenarios with radar observations". In: *CEAS Space Journal* (2022).

[3] Keric Hill, Chris Sabol, and Kyle T Alfriend. "Comparison of covariance based track association approaches using simulated radar data". In: *The Journal of the Astronautical Sciences* 59.1 (2012), pp. 281–300.

[4] Oliver Montenbruck and Eberhard Gill. *Satellite Orbits*. Vol. 1. Jan. 2000. ISBN: 978-3-540-67280-7. DOI: 10.1007/978-3-642-58351-3.

[5] ESA Copernicus. *Sentinel Online - Sentinel 3-A Orbit Description*. URL: https://sentinels.copernicus.eu/web/sentinel/missions/sentinel-3/satellite-description/orbit (visited on 01/03/2022).

[6] ESA Copernicus. *Sentinel Online - Sentinel 3-A Satellite Parameters for POD*. URL: https://sentinels.copernicus.eu/web/sentinel/technical-guides/sentinel-3-altimetry/pod/satellite-parameters (visited on 01/03/2022).